Feeling sugar-protein interactions using carbon nanotubes : a molecular recongition force microscopy study

Klein, D.C.G.

Chapter 7

Molecular recognition force microscopy on pea lectin and mannan binding lectin

This chapter describes the experiments that were made possible by combining all steps that were taken in the previous four chapters on our way to realize molecular recognition force microscopy with small ligands. Carbon nanotube AFM tips were functionalized covalently with a sugar molecule, as was described in Chapters 5 and 6. Pea lectin and mannan binding lectin, respectively, were immobilized on a surface according to the method described in Chapter 4.

Molecular recognition force microscopy studies were conducted with mannose-modified tips on pea lectin. Phase images show that the interaction between the modified tip and a protein is different from the interaction between the mannose-modified tip and mica.

The first experiments with mannose-functionalized multi-walled carbon nanotube tips on immobilized mannan-binding lectin provide strong evidence that specific binding has been observed in the phase images, with high resolution, allowing for sub-molecular imaging of binding sites.

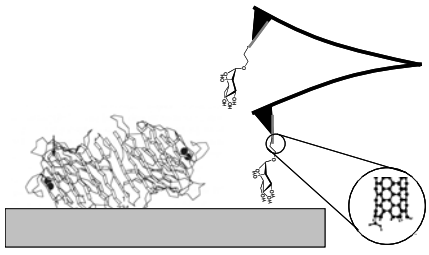

7.1 Introduction

The lateral resolution of molecular recognition force microscopy (MRFM) is primarily determined by the length of the spacer that couples the ligand to the AFM tip, as is shown in Figure 1.

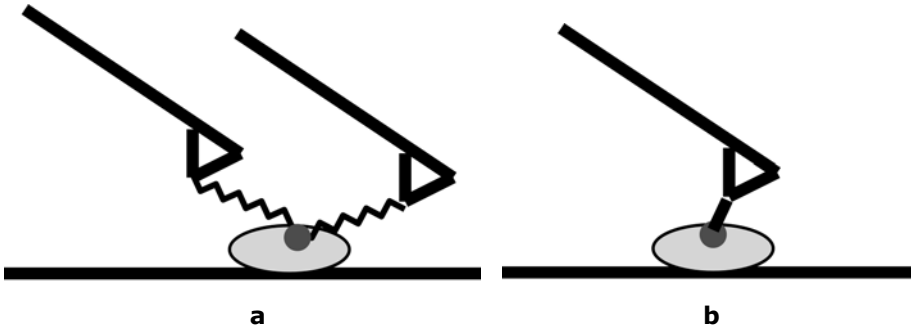

Figure 1 Long spacer versus short spacer: the resolution that can be obtained with chemically functionalized AFM tips is determined by the length of the spacer between ligand and tip. The sketch in (a) shows a polymer spacer, and (b) a nanotube spacer.

Using a long and flexible polymer as a spacer, as is commonly used in MRFM, the best resolution obtained is around 25 nm.[1] In order to improve the lateral resolution to 5 nm, which is a typical distance between binding pockets in a cluster of receptors on a membrane, we used a carbon nanotube as a spacer.

The development of carbon nanotube AFM tips was described in Chapter 5. We covalently bound mannose to a multi-walled carbon nanotube (MWNT) tip, as was explained in Chapter 6. Then we measured the interaction in liquid between this tip and a surface with either *Pisum sativum* lectin, PSL (§ 7.3), or mannan binding lectin, MBL (§ 7.4), which were immobilized on mica as was described in Chapter 4.

We expect to find information on the specific mannose-lectin interaction in the phase image, because the phase lag between the driving signal and the response of the cantilever on top of a binding site should be different from elsewhere on the protein. The phase is changed by the breaking of the bond which modifies the interaction potential as well as the dissipation. We start this chapter with a discussion of the interpretation of phase images and the influence of unbinding events. Then we present preliminary results on PSL and MBL that were obtained with MRFM with a short and stiff carbon nanotube as a spacer, which was functionalized with mannose.

7.2 Interpretation of phase images; qualitative and quantitative aspects

In tapping mode AFM, the cantilever is driven close to its resonance frequency. The response is determined by the cantilever properties such as spring constant and quality factor, as well as by the interactions between tip and surface.[2] The equation of motion for the oscillating tip is described by the following formula,

$$m\ddot{x} = -k(x - x_c) - b\dot{x} + F_{drive}(t) + F_{tip-sample}(x) \tag{7.1}$$

where m is the effective mass, x is the tip-surface separation, with equilibrium value $x_{c,}$ and k is the spring constant of the cantilever. F_{drive} is the driving force exerted on the cantilever and $F_{tip\text{-}sample}$ is the interaction force between tip and sample. When the cantilever is immersed in liquid, both m and b increase. For a quality factor Q>>1, the cantilever damping b is

$$b = \frac{m\omega_0}{Q} \tag{7.2}$$

where ω_0 is the angular resonance frequency of the free cantilever. The driving force is described by

$$F_{drive} = F_0 \cos(\omega t) \tag{7.3}$$

where F_0 is the amplitude of the external driving force and ω is the angular frequency of the driving force. In the absence of interactions, a steady state solution exists of the form of a sinusoidal oscillation,

$$x(x_c, t) = x_c + A(\omega)\cos[\omega t - \varphi(\omega)] \tag{7.4}$$

where A is the amplitude of the cantilever oscillation and φ is the phase lag between drive signal and the measured cantilever response. In the presence of tip-surface interactions, for small amplitude, the solution changes to

$$x(x_c, t) = x_0(x_c) + A(\omega, x_c)\cos[\omega t - \varphi(\omega, x_c)] \tag{7.5}$$

where x_0 corresponds to the mean deflection of the cantilever. For larger amplitudes, significant deviations from the pure sinusoidal motion can occur, which can be described by a set of higher harmonics.

The influence of tip-surface interactions on the deflection, phase and frequency of an oscillating cantilever have been exploited to gain understanding about intermolecular forces.

Van Noort has shown that the deviations from the pure sinusoidal motion, as described above, are different when scanning on top of a DNA molecule compared to scanning on mica that was covered by polylysine.[3] The motion has been described using a simple model of a damped, harmonic oscillator (see also Equation 7.1).

Excellent agreement has been found between theory and experimental results, using measured parameters such as k, ω_0, Q and the tip radius. Ashby developed elegant methods for the AFM, using well-defined tips and surfaces, to study intermolecular forces.[4]

In frequency modulation force spectroscopy, the shift in eigen-frequency of an oscillating cantilever is measured while scanning, which is a very accurate measure of the interaction force between tip and sample.[5]

In the references mentioned above, the tip-sample interaction contains a Van der Waals-type component and an electrostatic component. In our case, the specific interaction between sugar on the tip and lectin on the surface also plays an important role.

The phase lag φ changes with position on the sample during scanning, and can be shown in a phase image. Phase images contain information about adhesion and viscoelastic properties, or more generally stated, about energy dissipated in the tip-sample contact.[6]

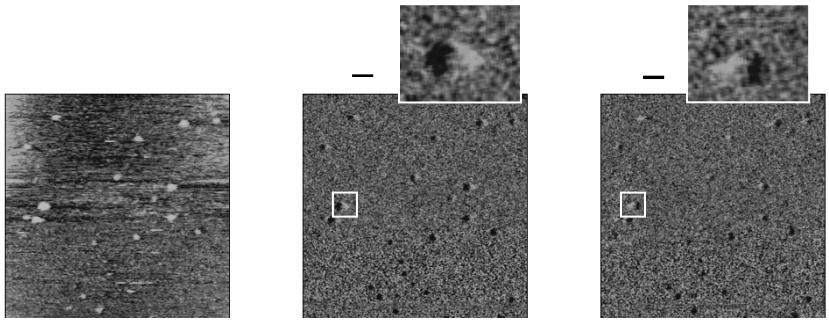

Figure 2 Mannose MWNT tip on PSL on mica in Tris buffer: (a) height trace (b) phase, trace (c) phase, retrace. Scales are 1 µm x 1 µm x 10 nm (a) x 29° (b) and x 30 ° (c). The scale bars in the zoomed regions are 25 nm. Images are low-pass filtered. By comparing the trace and retrace phase image, the influence of the topography on the phase contrast can be distinguished.

An important unwanted contribution to the phase image arises from the fact that a change in tip oscillation amplitude during scanning is also detected as a phase change.

$$\delta\varphi_{topo} \propto \frac{\partial A}{\partial t} \tag{7.6}$$

Such changes in the amplitude are induced by variations in the height of the sample. An example is given in Figure 2. In the phase image that was recorded from left to right (trace), see Figure 2 b, the molecule is dark on the left side (negative phase shift) and bright on the right side (positive phase shift). In the phase image that was recorded from right to left (retrace), see Figure 2 c, the molecule is dark on the right side, and bright on the left side.

Important to mention here as well is that the energy dissipation, and thus the phase response, varies significantly with both the driving force and the set-point tapping amplitude.

In addition to the topographic contribution, which may be large, depending on how large the amplitude variations are, the

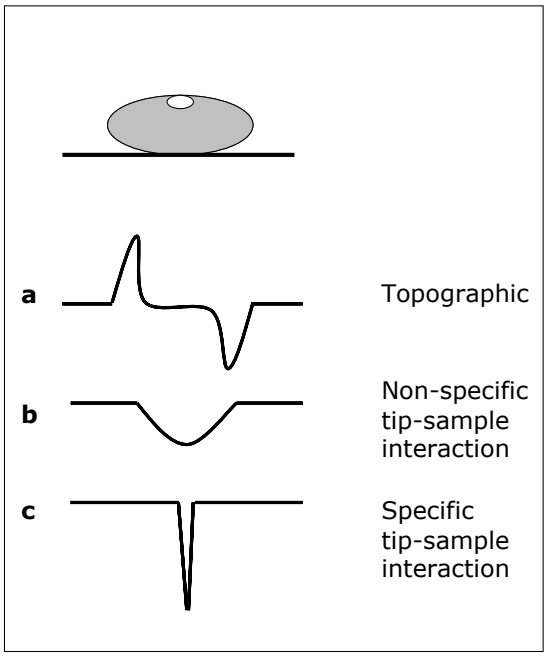

Figure 3 Diagram of the three contributions to the phase on a molecule with one binding site. The "sharpness" of the specific interaction depends on the length of the spacer.

changes in tip-sample interaction, both specific and non-specific, contribute to the phase image.

A sketch of what we might expect from these three contributions is shown in Figure 3.

A way to decompose the phase image into moments of topography and tip-sample interaction is described and applied to AFM images of purple membrane by Stark *et al.*[7] By correcting the phase image for influences of the error image and the interaction area, the image of the dissipative interaction energy density is obtained, which characterizes sample properties.

MRFM with short spacers: how to detect unbinding events

A very important difference between MRFM using long spacers, e.g. by Raab *et al.*,[8] and MRFM with short spacers, as used in our case, is the contact time between the functionalized tip and the receptor on the surface. In the long spacer case, the tapping amplitude is smaller than the spacer length, which implies that the ligand is specifically bound to the receptor for many tapping periods, before a rupture takes place. With a long spacer, the ligand is bound to the receptor during the complete scan of the tip over one receptor. In the short spacer case, however, rupture of the bond between ligand and receptor takes place during each tapping cycle. Whereas a ligand on a long spacer typically has several milliseconds to bind the receptor, a ligand on a short spacer typically only will have tens of microseconds to bind the receptor. This implies that the ligand may not bind the receptor each time the tip reaches the sample and detection has to be much faster in the short spacer case. Fortunately, each unbinding event effectively influences some (Q) of the following oscillations, which makes it more probable to be detected.

In the next section (§7.3), MRFM on pea lectin with mannose functionalized carbon nanotubes is demonstrated and discussed. At the end of §7.3, a new method for detection is suggested. In §7.4, first results of MRFM on mannan binding lectin are presented.

7.3 *Pisum sativum* lectin

Pisum sativum lectin (PSL) is a sugar binding protein from pea. Its biological function was described in § 3.3. PSL is a dimer with two binding sites for mannose that are around 5 nm apart, as was shown in Figure 9 in § 6.5. The equilibrium constant of specific binding of PSL with mannose is 1 mM.[9]

Experimental details

PSL was kept at 4 °C in a 0.1 M Tris buffer (Tris (hydroxymethyl) aminomethane) at pH 7.2. Mica was modified as was described in Chapter 4. A drop of 75 µl of PSL (1 µg/ml) in 0.1 M Tris at pH 7.2 was centrifuged for 5 min at 13000 rpm to remove large aggregates, and the supernatant was sonicated for 3 sec before application to the mica. After three hours of incubation, the excess of PSL was rinsed off, and the sample was imaged in 0.1 M Tris, pH 7.2. Two types of cantilevers were used: silicon cantilevers with a spring constant of 2 N/m and a resonance frequency of around 30 kHz in liquid (Figure 4, 5 and 8), and gold coated, thin silicon nitride cantilevers, with a spring constant of 0.03 N/m and a resonance frequency of around 7 kHz (Figure 6 and 7). On both types of cantilevers, multi-walled carbon nanotubes (MWNTs) were mounted as was described in Chapter 5. These nanotube tips were then chemically functionalized with mannose, as was described in Chapter 6. For the control experiments, a 0.1 M Tris buffer containing 20 mM mannose was used.

In air

Although, presumably, a protein needs to be in liquid to preserve its optimal binding activity, we probed the interaction between mannose on a nanotube tip and PSL in air, because even when in air, the protein will still be covered by a thin film of water. This thin layer might, or might not be enough to allow for specific binding between the sugar on the tip and the protein on the sample. We probed the interaction between a non-modified AFM tip and PSL on mica, as well as the interaction between a mannose-modified AFM tip and PSL on mica, both in air.

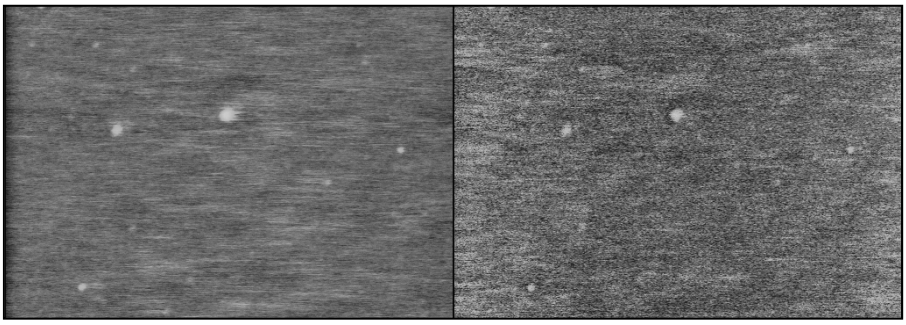

a **b**

Figure 4 Pea lectin on mica, imaged in tapping mode in air with a non-modified SiO_2 AFM tip. Shown are height (a) and phase (b). Scales are 470 nm x 325 nm x 3 nm (a) and x 20 ° (b).

The phase response on top of a protein is + 8 ° in the first case, as is shown in Figure 4 b, which means that the phase lags behind more on the mica than on the protein. The non-modified AFM tip did not contain a carbon nanotube.

In the second case, with the MWNT tip modified with mannose, the opposite occurs. The phase lags behind 8 ° more on the protein than on the mica, as shown in Figure 5 b.

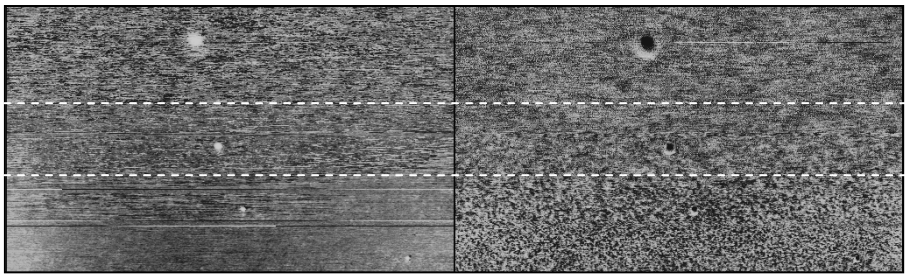

a **b**

Figure 5 Pea lectin on mica, imaged in air with a mannose modified MWNT-AFM tip. Shown are height (a) and phase (b). The grey scales span 3 nm (a) and x 20 ° (b). The protein is imaged three times with a different scale (zoomed during imaging), ending with an image width of 500 nm x 290 nm at the upper half. Notice the central region of negative phase shift (dark) surrounded by a ring of positive phase shift (bright) on the protein.

It is possible that the difference in phase response as shown in Figure 4 and 5 is caused by a non-specific interaction in the first case and a specific interaction, followed by an unbinding event in the second case. The interaction might also be of another nature: the interaction between the tip (which is hydrophylic for SiO_2, and hydrophobic for carbon) and the water layer on the surface, as was discussed in § 5.3.

In liquid

We found that in liquid the phase shift on PSL, when using a mannose MWNT tip, lags behind an additional 14 °, relative to mica, as is shown in Figure 6.

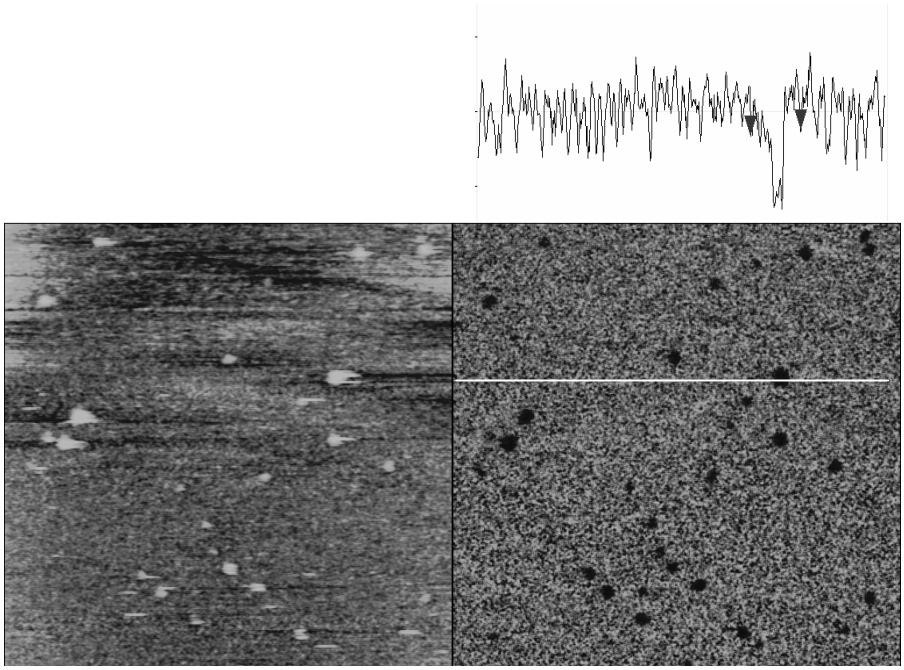

a **b**

Figure 6 Height (a) and phase (b) image of PSL immobilized on mica imaged with a mannose MWNT tip (k=0.03 N/m) in liquid. Scales are 1 µm x 1 µm x 10 nm (a) and 1 µm x 1 µm x 30 ° (b). The image has been low-pass filtered. The inset shows a line scan taken at the position of the white line.

After adding free mannose to the solution on the sample (mannose concentration 20 mM in Tris buffer, incubation time 30 min), as a control, the relative phase shift changed, as is illustrated in Figure 7. Notice that on a protein the contrast changed from dark (Figure 6) to bright (Figure 7). In Figure 7, the phase signal on a protein increased first, followed by a sudden decrease. It is therefore hard to determine the average phase shift on the protein. This is caused by the topographic influence on the phase, as was shown in Figure 3 a.

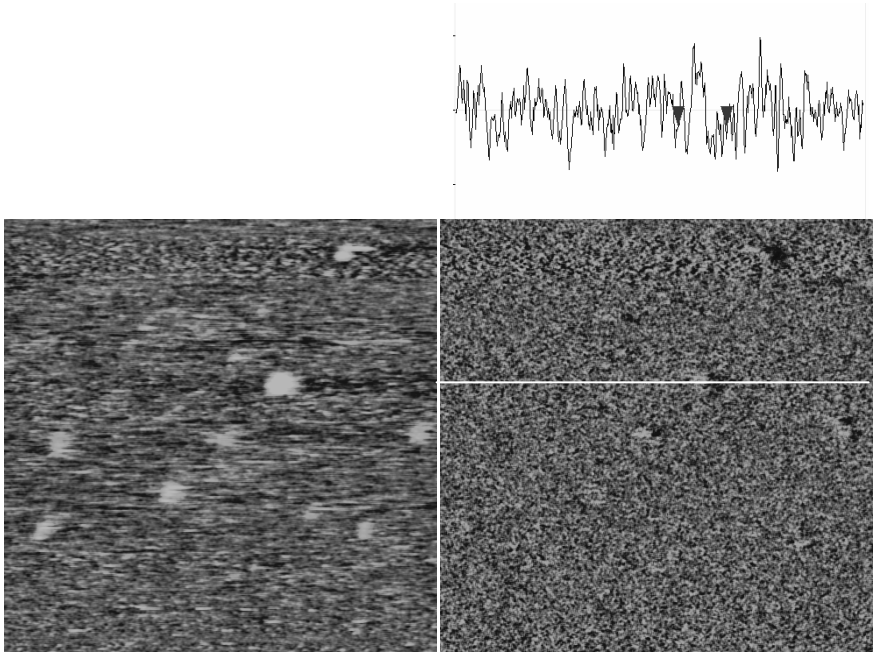

Figure 7 Control experiment: the same sample and mannose-tip as in Figure 6, but with free mannose in solution (20 mM) in order to block the mannose-binding sites in PSL. Height (a) and phase (b) image of PSL immobilized on mica imaged with a mannose MWNT tip (k=0.03 N/m) in liquid. Scales are 1 µm x 1 µm x 10 nm (a) and 1 µm x 1 µm x 30 ° (b). The image has been low-pass filtered. The inset shows a line scan taken at the position of the white line.

MRFM with short spacers: how to detect unbinding events, part II

It is possible that even though an unbinding event takes place, this will not show up in the phase image, as each pixel in the phase image is the average of the phase of tens of taps (depending on scan speed and resolution). If we assume that the lateral resolution is 5 nm with our short spacers, what is the consequence of this for the phase image?

Obviously, in order to prevent that the important information is averaged out, the pixel size should be chosen to be 5 nm or less.

Furthermore, because of the short linker, we expect unbinding only when the sugar is exactly (within 5 nm) on top of the binding site in order to be able to establish specific binding (followed by unbinding). For a cantilever with a resonance frequency of 30 kHz,

and a tip speed of 8 µm/sec, the tip has a chance to bind to the PSL only during 20 taps while scanning the binding site.

Finally, the probability that the sugar molecule binds to the binding pocket will be smaller than 1, because we do not expect that the position of the sugar on the tip will always allow for binding. This brings us back to the problem that the unbinding events possibly do not show up in the (averaged) phase, measured by a lock-in amplifier.

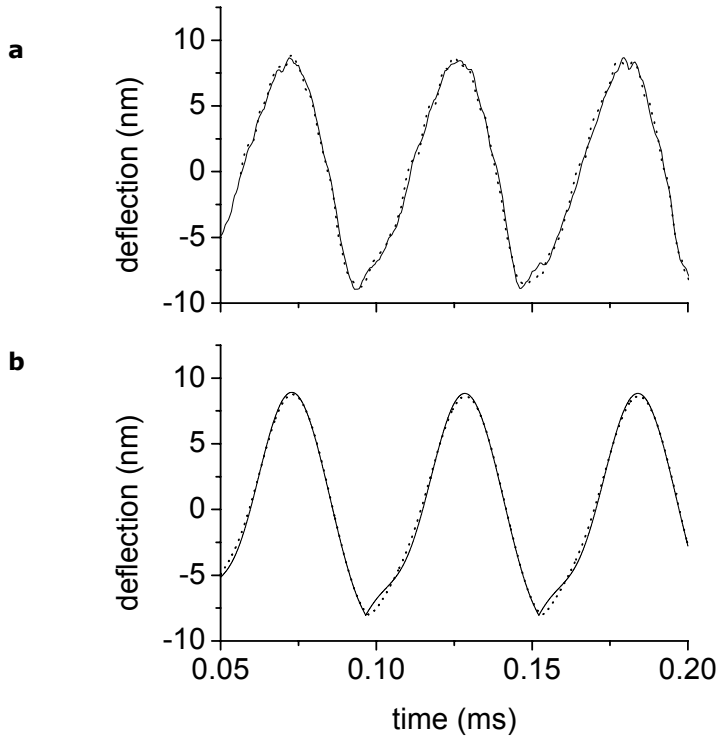

Figure 8 (a) Measured deflection traces of the cantilever tapping on poly-L-lysine coated mica (solid lines), and on DNA (dotted lines). (b) Shows the corresponding calculated traces. With permission of John van Noort, Reference 3.

In order to prevent loss of information in an averaging procedure such as performed by the Digital Instruments software, the complete tapping motion of the cantilever can be recorded, and compared to the driving signal. Van Noort has recorded the tapping motion of an unmodified AFM tip on DNA (negatively charged) absorbed on polylysine-coated mica (positively charged), and he found that differences in charge density cause subtle differences in the cantilever movement, as is illustrated in Figure 8.

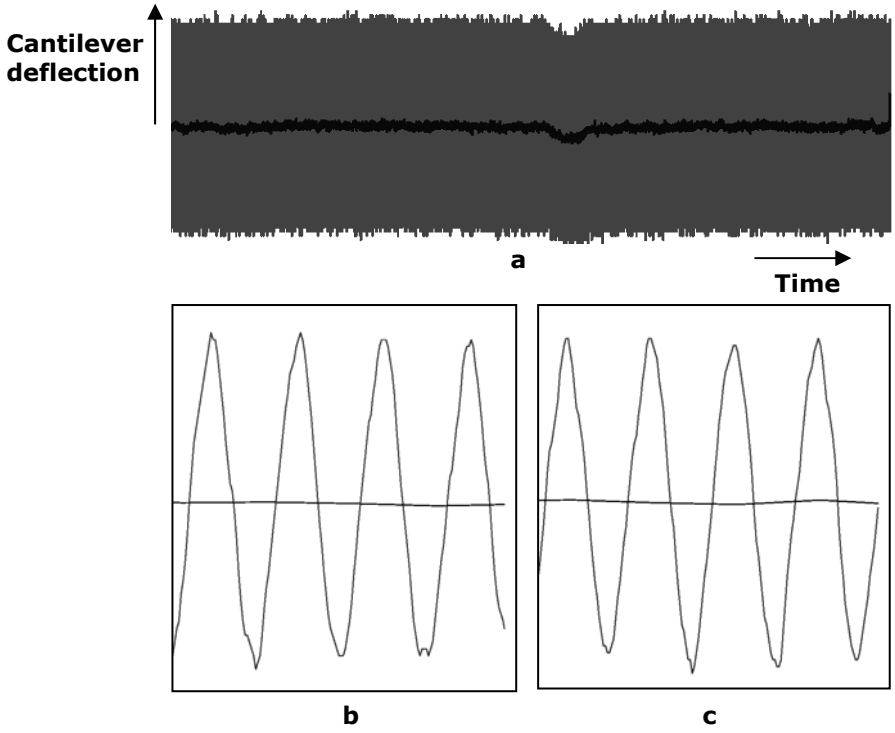

Figure 9 Cantilever tapping motion as a function of time. The black line in (a) is the average motion. The dip in deflection corresponds to a protein present on the mica surface. In (b) and (c) zooms of (a) are shown, recorded on mica (b) and on top of a protein (c). In (a) 30000 tapping periods are shown, so only the envelope of the oscillation can be seen.

We expect that the shape of the tapping motion should be different in the case of an unbinding event, when compared to tapping either on mica or parts of the protein that are not in the vicinity of a binding site. The upswing will probably be affected more by the specific binding than the downswing, and the phase lag will also change during unbinding.

We recorded the cantilever deflection using fast electronics, as is shown in Figure 9. The frequency of the cantilever was 30 kHz, and the number of points per period was 100, so 3 megasamples per sec were recorded. Interestingly, the offset of the cantilever deflection changes with respect to mica when the tip encounters a protein on the mica. Processing of these data is still in progress, and suggestions on how to analyze these data are given in Chapter 8.

Another way to improve the time resolution of the amplitude measurement without accumulating as much data, is detecting the position of the maxima and minima in the cantilever tapping. Special electronics were developed for this purpose.[10]

7.4 Mannan binding lectin

We also studied a lectin that is present in the blood stream of mammals: mannan binding lectin (MBL). Mannan is a polysaccharide of mannose. MBL plays an important role in the innate immune system. It recognizes sugar patterns on the cell wall of bacteria and other micro-organisms, and can detect these invaders even before the classical pathway of antigen-antibody interaction has started to work. MBL is an oligomer made up of two to six subunits. Each subunit is composed of three identical polypeptide chains that are wrapped around each other like in collagen. Each subunit contains three sugar-binding sites. Subunits are linked through sulfur bridges that form between subunits at the end region of the collageneous structure. A sketch of the molecular structure of MBL is shown in Figure 10.

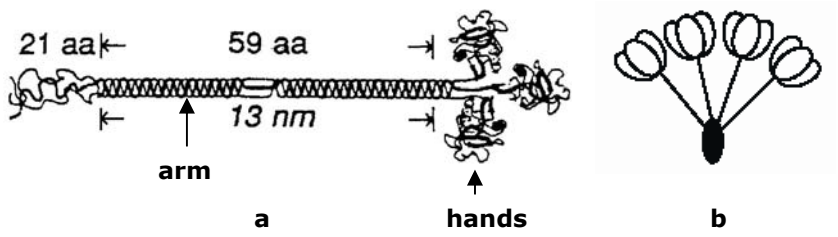

Figure 10 (a) Sketch of a single subunit of MBL, consisting of three identical polypeptide chains containing a long collageneous region (arm) and a globular region (hand) with a sugar binding site. (b) Molecular structure of a tetramer of mannan binding lectin (MBL). Looking at it as if it were a bunch of flowers, the flowers represent the sugar binding sites (three for each flower), the stems are the collageneous region, and they end in a hub that links the stems together. The distance between the mannan binding pockets is ~ 5 nm.

MBL binds to mannan with an equilibrium constant of 2 nM, and to mannose, albeit with a lower affinity, with an equilibrium constant in the mM range.[11] In order to be able to specifically bind mannose or mannan, MBL has to be in a calcium rich environment.

Experimental details

First, the control measurement was done in a 50 µl drop of TBS (10 mM, 150 mM NaCl) containing 3 µg/ml recombinant MBL. Then, 4 µl $CaCl_2$ (100 mM) was added, and after 20 min the experiment was continued.

MBL was kept at 4 °C in TBS (10 mM, 150 NaCl). The imaging buffer without calcium also was 10 mM Tris, 0.15M NaCl. MBL was anchored to mica as was described in Chapter 4.

Unfortunately, all buffers described here contain tracers of Ca^{2+} (80 nM). In order to reduce the Ca^{2+} concentration further, the controls without Ca^{2+} should be repeated in buffer containing several mM of EDTA, which binds Ca^{2+}.

A silicon cantilever with a spring constant of 2 N/m was used with a MWNT attached to the tip. The frequency at which the cantilever was driven was 29.2 kHz before addition of calcium and 29.4 kHz after addition of calcium. Re-adjusting the drive frequency was needed in order to drive the cantilever close to its resonance with approximately the same amplitude in both measurements. Gains were kept constant; tip speed was varied within a factor of two.

In air

In Figure 11, an AFM image is shown of MBL on mica,

Figure 11 Perspective representation of an AFM image of MBL, taken in tapping mode air with a silicon tip. Scales are 120 nm x 80 nm x 2.5 nm. The arms and hands are lying flat on the mica surface, and the hub sticks out of the plane (white dot). The image was recorded by Henriette Jensenius.

recorded in air. Individual MBL complexes were clearly resolved. The arms and hands lie flat on the mica and the hub points up.

Preliminary experiments in liquid

An AFM image taken in liquid of MBL is shown in Figure 12. MBL was immobilized covalently on mica, as was described in Chapter 4. The resolution is far worse than that in air, because the protein complexes are only immobilized by one, or at most two or three linkers. This is because of the limited density of linkers on the mica. The mannan binding sites should be accessible for the tip.

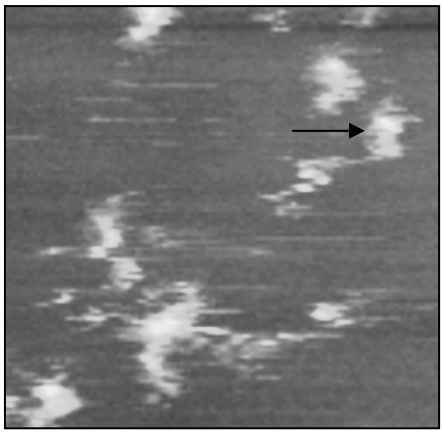

Figure 12 MBL immobilized covalently on mica, imaged with a mannose nanotube tip in a buffer solution without calcium. Scales are 250 nm x 250 nm x 5 nm. The arrow points at a single MBL molecule, with the collageneous tail sticking up and the arms with sugar binding sites at the end lying flat.

We imaged MBL using a multi-walled carbon nanotube (MWNT) tip that was functionalized with mannose. The measurements were performed in a calcium rich buffer solution, where the binding activity of MBL is preserved. Local phase lag ("dark spots") can be seen in the phase image, on parts of the protein, as is shown in Figure 13 a. We ascribe this remarkable phase behavior to the specific interaction between sugar on the tip and active MBL.

As a control, measurements were also performed in a buffer without added calcium. In the absence of calcium, MBL can not specifically bind mannose or mannan. These results are shown in Figure 13 b. Far fewer black dots were observed in this case compared to Figure 13 a. The fact that we still observed some events, can be explained by the following. The concentration of calcium in the buffer that we used in the control experiment can still be as high as 80 nM [12], because this is the concentration of calcium in deionized water. For a number of approximately $0{,}4 * 10^{12}$ MBL binding sites on the surface, this calcium concentration is sufficient to make all MBL complexes active (approximately $2 * 10^{12}$ calcium ions present). The proper way to conduct this control would have been to measure in a buffer containing 2mM EDTA, in order to make sure that it would be really calcium-free.

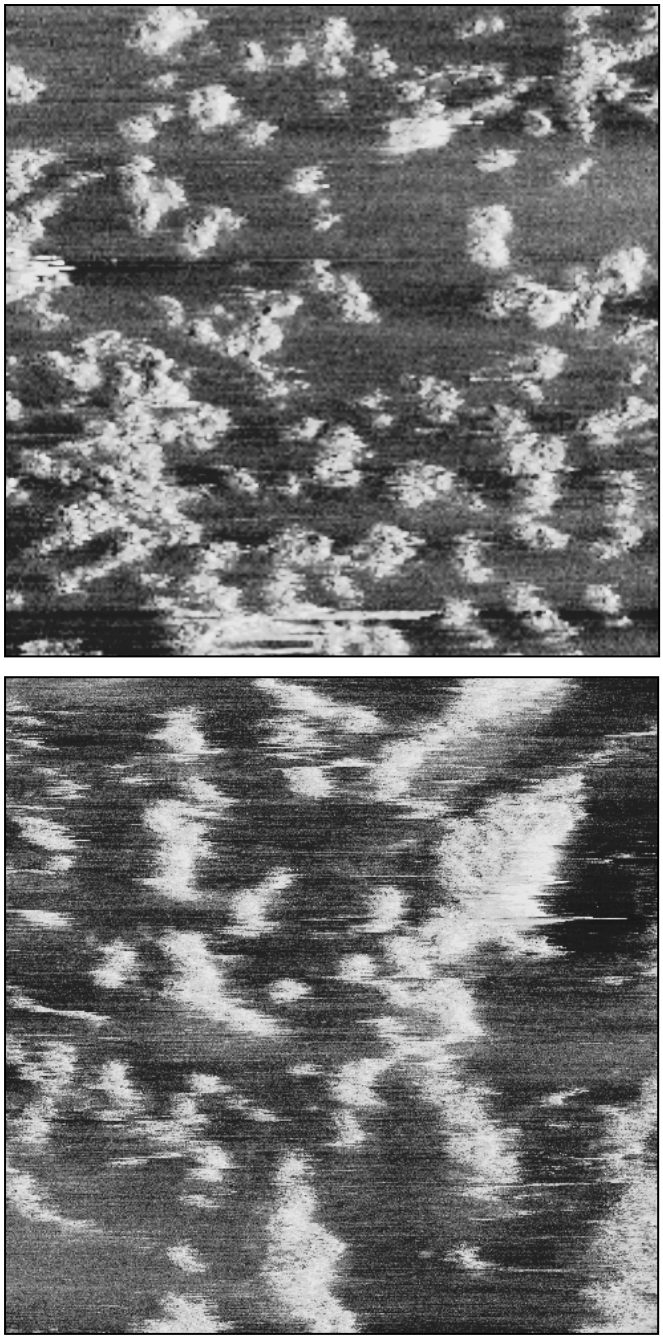

a

b

Figure 13 Mannan binding lectin imaged with a mannose-MWNT tip in tapping mode in a buffer solution WITH (a) and WITHOUT (b) calcium. Shown are phase images (both trace). Scales are in both cases 1 µm x 1 µm x 20 °. In (a), many dips can be seen on the lectin, while in (b) only very few black dots can be distinguished. In a, a software zoom of an AFM image of 2 µm x 2 µm is shown.

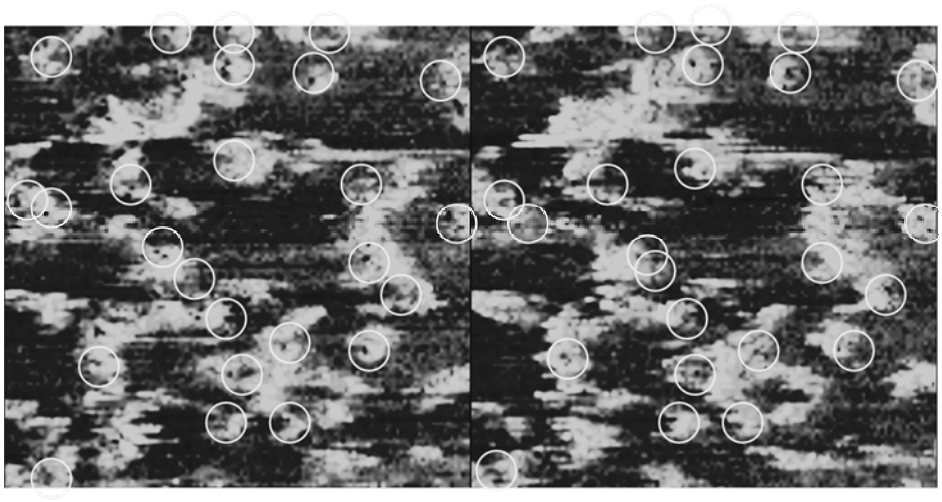

a **b**

Figure 14 Phase images of MBL taken with a mannose-functionalized MWNT tip in tapping mode in Tris buffer containing calcium. (a) trace, (b) retrace. Software zoom of Figure 13. Scales are 500 nm x 500 nm x 10 °. 1 pixel = 4 nm.

Comparing trace and retrace images taken on MBL with a mannose-functionalized MWNT tip, we find that although the dark

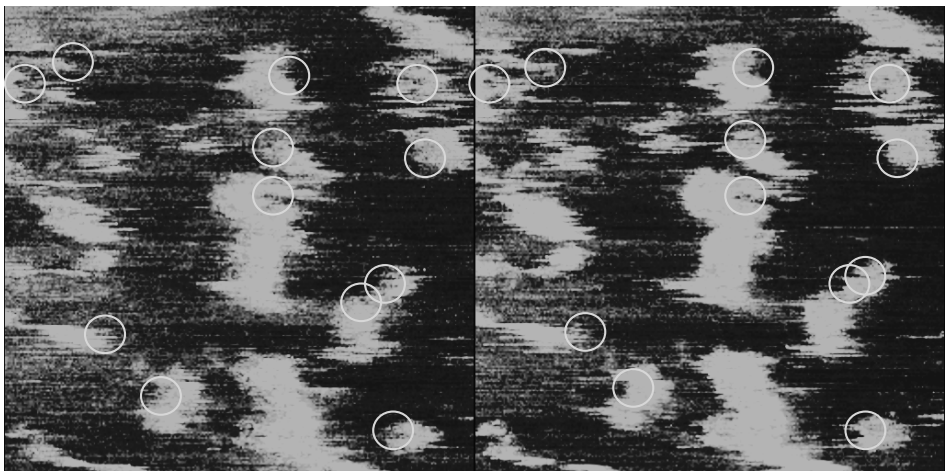

a **b**

Figure 15 Phase images of MBL taken with a mannose-functionalized MWNT tip in tapping mode in Tris buffer without calcium: (a) trace, (b) retrace. Software zoom of a 1 µm x 1 µm image. Scales are 500 nm x 500 nm x 10°. 1 pixel = 2 nm.

spots in the phase images do not overlap exactly, there is a high degree of correlation between the locations of the " dark spots" in the trace and retrace images: 25 times on an area of 500 nm x 500 nm. This is shown in Figure 14, which is a software zoom of Figure 13 a. Although we find fewer black dots in the control experiment, some are present in trace and retrace on the same part of the molecule (12 on an area of 500 nm x 500 nm), as can be seen in Figure 15.

Another important observation is that in several cases, the "dark spots" consist of more than one pixel (in the original image), which implies that in two or more subsequent scan lines the same response in the phase occurred on the same part of the molecule. In the control experiment, this happened 14 times in an area of 500 nm x 500 nm, as can be seen in Figure 16 a. This should be compared to 27 times in the experiment with calcium present in the buffer, as can be seen in Figure 16 b.

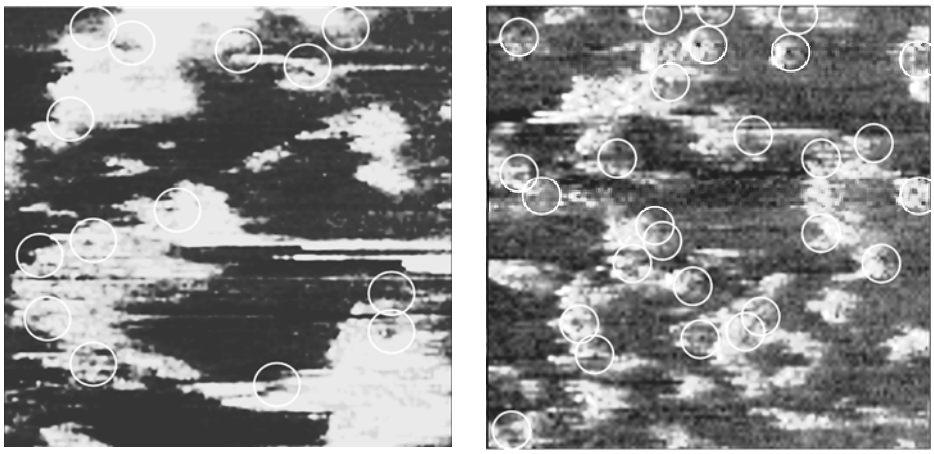

no calcium added with calcium

a **b**

Figure 16 Phase images of MBL taken with a mannose-functionalized MWNT tip in tapping mode in Tris buffer (a) without and (b) with calcium. Scales are 500 nm x 500 nm x 10 °. In this image the dark spots are circled that consist of several pixels, which means that the phase response was the same on the same spot in the next line. 1 pixel = 4 nm.

How many binding sites per molecule do we expect? Each MBL has between two and six arms, and each arm has three hands. Each hand contains one sugar binding site, which implies that per molecule we expect between 6 and 18 binding sites. The density of molecules on the surface is approximately 20 %. The area per molecule is approximately 700 nm^2. Per image, we expect to have approximately

70 MBL molecules. This corresponds to between 420 and 1260 binding sites. We detected around 25 binding sites, which is far less. One reason could be that not all binding sites are accessible, because of the orientation of the molecules on the surface. Also, unbinding events on the side of an MBL complex can be "missed" because of the large change in height and the corresponding change in amplitude. As was discussed in § 7.2, dA/dt has a large contribution to the phase. Another reason for this difference is that the position of the sugar should be such that it can enter the binding pocket, which we do not expect to be true for each attempt, as was discussed in § 7.3.

In order to be able to quantify the results shown above, several additional data analysis tools need to be developed. First, a correlation procedure should be defined, which automatically distinguishes unbinding events from noise, by searching for correlated "spots" of deviating phase. The number of unbinding events in both cases (no calcium and calcium) should be compared. This should be done both in trace and retrace images, in order to find if binding sites are consistently found in trace and retrace images.

7.5 Conclusions

We performed molecular recognition force microscopy, using multi-walled carbon nanotube tips that were functionalized with mannose on two different kinds of sugar-binding proteins: pea lectin and mannan binding lectin.

MRFM images on pea lectin in air show different phase contrast compared to a phase image that was recorded with a non-modified AFM tip. We tentatively ascribe this to specific interaction between mannose on the tip and pea lectin. It is not known, however, whether specific binding can be detected when measurements are performed in air. Possibly, the thin water layer that is present on the molecule allows specific interaction.

The difference in phase contrast was also observed when measurements were performed in liquid. A control experiment by adding free mannose to the buffer solution, in order to block the binding sites, shows a phase contrast that is lower and contains a large topographic contribution. This strongly suggests that the phase contrast is caused by specific mannose-lectin interactions.

MRFM on mannan binding lectin in a buffer solution containing calcium shows a difference in phase behavior on different spots within one MBL complex. On these images with a 4 nm pixel size, we find signals that are either one or two lines wide so we can safely assume the resolution is better than 8 nanometer. As a control, MRFM was also performed on MBL in a buffer solution without calcium, which decreases the specific binding activity of MBL. In this case, comparable phase behavior was found, but less unbinding events

were detected. This strongly suggests that the interaction that we found is caused by specific interaction between mannose and MBL.

To get a reliable measure of the resolution it is necessary to take scans at a larger magnification, to decrease the pixel size. Also, the scan speed should be chosen low enough in order to allow many "taps" of the tip in the vicinity of the binding site.

We developed high-resolution MRFM for small ligands, in our case sugars. This method can be applied to study the binding function of receptors on a single-molecule level.

---

[1] Raab, A., Han, W., Badt, D., Smith-Gill, S.J., Lindsay, S.M., Schindler, H., and Hinterdorfer, P. Antibody recognition imaging by force microscopy, Nature Biotechnology **17** (1999), 902-905

[2] San Paolo, Á., and García, R., Unifying theory of tapping-mode atomic-force microscopy, Physical Review B **66** (2002), 041406R

[3] Noort, S.J.T. van, Atomic force microscopy of dynamic protein DNA interactions, PhD thesis Twente University (1999)

[4] Ashby, P.D., Intermolecular and interfacial forces: Elucidating molecular mechanisms using chemical force microscopy, PhD thesis Harvard (2003)

[5] Sader, J.E., and Jarvis, S.P., Accurate formulas for interaction force and energy in frequency modulation force spectroscopy, Applied Physics Letters **84** (2004), 1801-1803

[6] Cleveland, J.P., Anczykowski, B., Schmidt, A.E., and Elings, V.B., Energy dissipation in tapping-mode atomic force microscopy, Applied Physics Letters **72** (1998), 2613

[7] Stark, M., Möller, C., Müller, D.J., and Guckenberger, R., From images to interactions: High-resolution phase imaging in tapping-mode atomic force microscopy, Biophysical Journal **80** (2001), 3009

[8] Raab, A., Han, W., Badt, D., Smith-Gill, S.J., Lindsay, S.M., Schindler, H., and Hinterdorfer, P. Antibody recognition imaging by force microscopy, Nature Biotechnology **17** (1999), 902-905

[9] Eijsden, R. van, Mutational analysis of pea lectin, PhD thesis Leiden University (1994)

[10] Peak-detection electronics were developed by Raymond Koehler

[11] Holmskov, U., Malhotra, R., Sim, R.B., and Jensenius, J.C., Collectins:collagenous C-type lectins of the innate immune defense system, Immunology Today **15**-2 (1994), 67-74

[12] Information from Elga Ltd.,High Wycombe, Bucks, England